Oxygen Evolution and Reduction Reaction Activity Investigations on Fe, Co or Ni embedded Tetragonal Graphene by A Thermodynamical Full-Landscape Searching Scheme

Yanqin Gai*[a]

Single transition metal (TM) atoms such as Fe, Co and Ni occupying a carbon divacancy in tetragonal graphene (TG) and bonded with four nitrogen atoms (TM@N_4TG) as electrocatalysts are investigated by means of first-principles calculations. To consider the effect of solvent species on the local configuration of the active single metal, a thermodynamical full-landscape searching (TFLS) scheme is employed. The calculated thermodynamic overpotentials (η_{td}) from our TFLS indicate that Co@N_4TG displays high catalytic activity toward both oxygen evolution reaction (OER) and reduction reaction (ORR), with η_{td}^{OER} and η_{td}^{ORR} as 0.397 and 0.357 V, respectively. Its OER potential cannot be captured if only one four electron reaction loop (FERL) is considered. The actual active pathways do not always turn out to be the reactions starting from the ***bare*** site. Our findings demonstrate that TG is a promising support and TM confined TD can be used to design effective and cheap multifunctional electrocatalysts.

1. Introduction

Effective and inexpensive electrocatalysts for both oxygen reduction reaction (ORR) and oxygen evolution reaction (OER) play significant roles in developing novel energy systems such as reversible fuel cells, metal-air batteries, and water electrolyzers.[1] The OER and ORR occur at the anode of a electrochemical water splitting cell and at the cathode of the fuel cell and the metal-air battery, respectively.[2] It is generally accepted that catalysts such as noble metal ruthenium (Ru) and iridium (Ir) oxides, platinum (Pt) and its alloys are required to facilitate low over-potential and fast kinetics.[3] The scarcity of these noble metals, however, limits their wide application as electrocatalysts. It is highly desirable to search for non-precious metals as replacements. The electrocatalytic performance of single-atom catalysts (SAC) with transition metals embedded in two-dimensional (2D) materials for OER and/or ORR have been intensively investigated.[4] The SACs provide tunable numbers of active sites, maximize the utility of metal atoms and act as ideal test grounds for rational design of catalysts. The supporting 2D materials include most of the widely explored ones.[5] Many research work on SACs for OER and ORR are conducted on carbon materials as they exhibit excellent conductivity, low cost and are wide used in electrochemistry.[6] Recently, tetragonal graphene (TG), a 2D tetra-symmetrical carbon allotrope, has been predicted to be energetically and kinetically stable.[7] TG is more favorable in energy than graphyne and graphdiyne, although it is meta-stable against graphene.[8] It is a 2D sheet constructed by carbon octagons and squares alternatively. Moreover, the pristine planar TG sheet shows a metallic character, which will benefits TG for electrochemical catalysis.[9] Notably, the less stable graphyne and graphdiyne have already been obtained experimentally and explored as potential SACs for various reactions.[10] In this work, the potential of TG as a support material for SACs has been systematically investigated. In order to bind the large TM atom tightly, a double-carbon vacancy with four neighboring nitrogen atoms is created.[11] Transition metals Fe, Co and Ni are selected in our work as these common metals confined by other 2D materials exhibited high OER and ORR activities.[12]

Currently, considerable efforts have been devoted to screen ideal SACs computationally.[10b,13] The computational hydrogen electrode (CHE) method proposed by Nørskov et al is employed by almost all the theoretical investigations.[14] In this method, the ***bare*** metal atom is chosen as the active site * for adsorbing species O, OH and OOH firstly. Then the Gibbs free energy changes of forming intermediates *O, *OH and *OOH involving four electron and proton transferring are calculated. The thermodynamic over-potential (η_{td}) for OER and ORR η_{td}^{OER}/η_{td}^{ORR} are finally determined by the largest/smallest energy difference between this four-electron reaction loop (FERL). The electrocatalytic potential of TM confined by Graphene, graphite–CN, graphyne, graphdiyne, C_2N, C_3N and C_3N_4 are all studied by the conventional CHE scheme.[15] Generally, Co@2D exhibit electrochemical activity towards OER or/and ORR.[16] Nevertheless, considering only one FERL starting from the ***bare*** TM site, we found that none of the Fe, Co, Ni @N_4TG systems showed OER

[a] *Prof. Y. Gai*
School of Materials science and Physics
China University of Mining and Technology
Xuzhou, Jiangsu 221116 (China)
E-mail: yqgai@cumt.edu.cn

Supporting information for this article is available on the WWW under https://doi.org/10.1002/open.202000326

activity, only the Co@N_4TG exhibited ORR activity. In this scheme, the ***bare*** metal on the surface cannot describe the real the surface in the solvent solution. Some functional groups such as O, OH or OOH would adsorb onto the surface of the electrocatalyst.[17] Various investigations confirmed that the types and coverage of functional groups affected the catalytic activity significantly.[18] The simple surface structure renders SAC an ideal subject for exploring the OER/ORR catalytic mechanism. The confined TM might be pre-adsorbed by O, OH, OOH or their mixture with the applying of electrode potential and the configurations with the above species will be called the intermediate states (IS). Some intermediate states might be shared by multiple four electron reactions and hence connect these multiple reactions. In the present work, a thermodynamic full-landscape searching scheme (TFLS), which is an extension of the standard CHE method is employed. One first lists all possible intermediate states by adding one OH or removing one H from ***bare*** metal site * successively. Then one writes out all the FERLs according to the order of oxidation or reduction. Finally, the thermodynamic overpotential is determined by the criteria that no trap intermediate state (TIS) is observed along the whole reaction path when the applied voltage is minimum (for OER) or maximum (for ORR). A TIS means the Gibbs free energy of such a state ranks the lowest among all the other intermediate states, where it transits to or is formed from.

In this work, the electrocatalytic activities of single Fe, Co and Ni atoms embedded in the double-carbon vacancy site of the TG monolayer with four neighboring nitrogen dopants (TM@N_4TG) as shown in Figure 1 toward OER and ORR are systematically investigated by both the CHE considering only one FERL and our TFLS method. Different conclusions are presented by these schemes.

Computational Methods

All the calculations in this work were carried out at the spin-polarized density functional theory (DFT) level using the Vienna ab initio Simulation Package (VASP).[19] The projector-augmented wave (PAW) potential was employed to describe the electron-ion interactions.[20] The Perdew-Burke-Ernzerhof (PBE) functional within the generalized gradient approximation (GGA) was adopted to model the exchange correlation energy.[21] The electron wave-functions were expanded by plane-wave with a cutoff energy of 500 eV. All atoms were fully optimized by conjugated gradient algorithm with a convergence criterion for energy and force of 10^{-5} eV and 0.02 eV/Å, respectively. A $4\times4\times1$ supercell containing 64 atoms as shown in Figure 1 was used. A vacuum space of 20 Å was inserted along the normal direction to the 2D TG to avoid artificial interactions between the periodic images. The Brillouin zones of supercells were sampled with $3\times3\times1$ Γ-centered k-points. The DFT-D3 method was used to accurately describe the long-range van der Waals (vdW) interactions.[22] To consider the effects of water, the polarizable implicit solvent model was used as implemented in VASPsol with the dielectric constant set to 78.4.[23] The localized 3d electrons correlation for Fe, Co and Ni were described by considering the on-site coulomb (U') (denoted as U' to be distinguished from the applied electronic voltage U in the following discussions) and exchange (J) interactions and the corresponding U'-J values 3.29, 3.42 and 3.4 were used for Fe, Co and Ni in our DFT + U' calculations, respectively.[24] The details of calculating binding energy (E_b), formation energy of intermediate states and over-potential for OER/ORR in one FERL calculations are provided in the supporting information.

2. Results and Discussion

The geometry and stability of TM@N_4TG were investigated firstly. The calculated binding energies E_b of one TM atom to the single N_4TG layer were −3.243, −3.128 and −3.069 eV, respectively. These values are all negative and their absolute values are large implying that a strong chemisorption has been built between the TM atoms and the N_4TG substrate. Non-metal

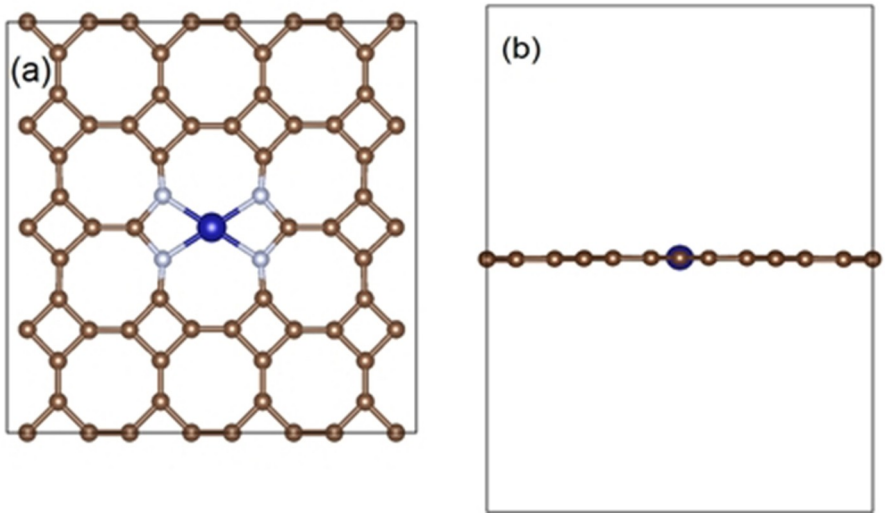

Figure 1. Top and side view of the optimized structures of one TM and four nitrogen atoms co-doped TG. The gray, blue and brown balls represent the N,TM (= Fe, Co, Ni) and C atoms, respectively.

atoms such as B, N, and O are generally employed to the decorated divacancy pores in graphene.[25] Among them, the N_4 divacancy pore (a divacancy with four neighboring nitrogen atoms) binds the divalent 3d TMs strongly because of the large enough pore size and the strong p-d hybridization between TM and nitrogen atoms.[26] Similar to TM@N_4Graphene, the TM atom remains within the basal plane of N_4TG after structural optimization (see Figure 1). Since the TM atom does not protrude from the doped surface, the upper and lower sides of the TM are equivalent. Under such circumstance, both side of the incorporated single TM atom serves as the active site to adsorb species such as O, OH and OOH. All the possible intermediate states (TM@N_4TGO_xH_y, $x=0\sim4, y=0\sim2$) are formed by either adding OH^- or removing H^+ to or from the bare TM@N_4TG successively. All the optimized structures of different intermediates are given in Figure S1. Two intermediate states are connected only when they can transit from one to another by either adding OH^- or removing H^+ from the system. All the FERLs formed by linking the intermediate states between neighboring oxidation states are shown in Figure S2. As can be seen from Figure S2 that since they share some common intermediate states, different FERLs might be coupled together. One intermediate state might be branched into several different oxidation states in the following steps. If any one of the branches contains a TIS, the whole system will fall into this TIS and eventually come to an end. The over-potential of the whole system is determined by the applied U that would remove all the possible TISs.

The intermediate states in Figure S1 are classified into different groups according to the number of electrons the electrode requires to form them. The maximum number of electrons is seven, and the corresponding intermediate state can be considered as the 7^{th} oxidation state. Therefore, the formation energies of these intermediate states will depend on the applied electrode potential as *-i*U*, where *i* is the number of transferred electrons. As will be shown later, the formation energies of all the intermediate states shown in Figure S1 are used to determine the over-potential for the whole reaction in our TFLM.

Next, the catalytic activity of the three TM@N_4TG catalysts for OER and ORR were systematically investigated.

The free energy diagrams for the eight FERLs on Co@N_4TG under $U=0$ V were shown in Figure 2(a)–(h) and were used to evaluate the catalytic performance of Co@N_4TG for OER and ORR. In each diagram, the uphill steps indicate the OER and the opposite process represents the ORR. Figure 2(a) gives the FERL starting from the ***bare*** Co site, which is the conventionally investigated FERL in the CHE scheme and here it is presented for comparison. The calculated η_{td}^{ORR} and η_{td}^{OER} for Loop a and Loop a' (the reverse process of Loop a) are 0.357 and 0.604 V, respectively. These values indicate that Co@N_4TG shows excellent ORR performance but is not suitable for OER. Poor catalytic activities of Co@2D for ORR have also been identified on Co@C_9N_4, Co@C_2N and Co@phthalocyanine, excellent bifunctional electrocatalysts for OER and ORR, however, have been confirmed on Co@N_4Graphene and Co@C_3N by computational investigations.[15e][27]In heterogeneous catalysis, the influence of the pre-adsorbed species from solution on the catalytic reaction on the metal active site ought to be considered.[17b][28] Given above situation, a whole reaction loop involving eight successive FERLs including intermediates *,*OH,*O,*OOH,*1O1O-H,*1O1OOH,*1OH1OOH,*2OH,*2O and *2OOH is generated. According to these individual FERLs in Figure 2(a-h), the smallest η_{td}^{OER} (0.349 V) is obtained from Loop d. The largest energy differences in Loop d is 1.579 eV, which comes from the transition from *1O1OOH to *2OOH. This means all the steps in Loop d will be exothermic when an electrode potential of 1.579 V is applied. However, we note that the *1O1OOH state in Loop d is shared by Loop c, g and h. Such a common intermediate state might lead reaction to proceed away from Loop d. The real reaction mechanism ought to be investigated by a full-landscape searching scheme. The free energy diagrams for a whole reaction loop containing all the successive FERLs on Co@N_4TG under different potentials are given in Figure 3 (a) and (b), which were called the TFLS plots and were used to derive the wholesome over-potential. Each TFLS plot combines eight individual FERLs indicated by different colors and the active FERL (not definitely the active loop of the whole reaction) was highlighted by the bold lines. The FTLS plot in Figure 3(a) shows that when the reaction arrives at *1O1OOH (at 5e), it prefers to proceed towards *O (at 6e) along Loop c, g and h, given that these pathways are more energetically favorable. Among the three FERLs, Loop c starts from *O (at 2e) and becomes *1O1OH (at 3e). An additional energy of 40 meV, however, is needed if it continues to its third step *1OH1OOH (at 4e). The *1O1OH (at 3e) turns out to be a TIS for Loop c, which means the whole process would be trapped by *1O1OH at 3e and come to an end after times of recycling. Similarly, the *O state (at 2e) in Loop g would also be a TIS since the transition from *O (at 2e) to *OOH (at 3e) is energetically unfavorable. The TIS *1O1OH (at 3e) for Loop h is also observed as the energy of *2O (at 4e) is 0.543 eV higher than that of *1O1OH (at 3e). One can see from above finding that, in terms of an individual FERL, Loop d is active under the oxidation electrode potential of 1.579 V. Such a potential, however, cannot render the whole reaction free of TIS since multiple FERLs occur successively. A higher applied potential U is required to avoid TISs. As Figure 2 (a-h) shows Loop b, c and f are all active individuals at a larger U of 1.627 V. The corresponding TFLS plot at $U=1.627$ V is given in Figure 3(b). As can be seen from Figure 3(b), starting from *O (at 2e), Loop c goes to *1O1OH (at 3e) and then to *1OH1OOH (at 4e). Since it shares the same intermediate state *1OH1OOH (at 4e) as Loop b, a much larger energy drop of 0.861 eV in Loop b drives the reaction to go towards $*OH+O_2$ (at 5e) along Loop b; Loop f starts from *OH (at 1e) and proceeds towards *2OH (at 2e) since it shares the common intermediate state *OH (at 1e) as Loop b and the *2OH (at 2e) is about 0.163 eV lower than *O (at 2e). The *2OH (at 2e) happens to be the second step of Loop b and no TIS is observed for Loop b. Hence, we conclude that the whole OER reaction on Co@N_4TG goes along the most energetically favorable Loop b with the lowest η_{td}^{OER} of 0.397 V, and the rate-determining step is the third one from *1O1OH to *1OH1OOH. The single metal centers are bonded with four N

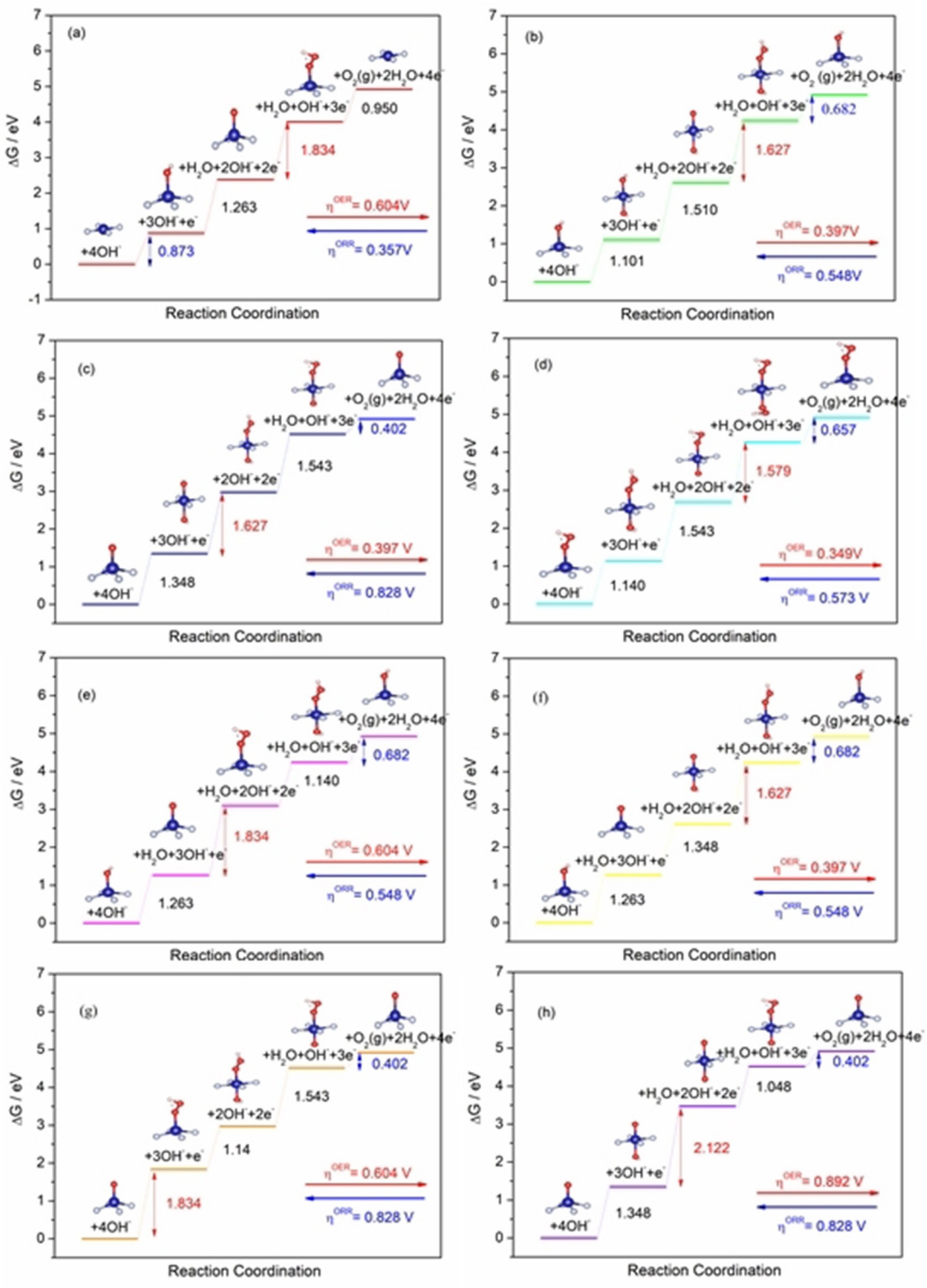

Figure 2. The free energy diagrams for all the eight FERLs (a-h) on Co@N_4TG under U = 0 V. The potential-determining step of the elementary reaction was marked by line with arrows. The local structures of the active Co site are shown on each step. The gray, red, pink and blue balls represent the N, O, H and Co atom, respectively.

atoms and one O atom in the first coordination sphere, which were also obtained by X-ray adsorption near-edge structure (SANES) simulation in TM@N_4Graphene system.[29]

The contrary reactions of the eight individual OER FERLs in Figure 2(a-h) represent the eight ORR FERLs (from Loop a' to Loop h'). Among them, the lowest η_{td}^{ORR} of 0.357 V was observed from Loop a', indicating all the elementary steps of Loop a' are exothermic or adiabatic when the system is applied by a reverse potential of 0.873 V. Similar to OER, whether Loop

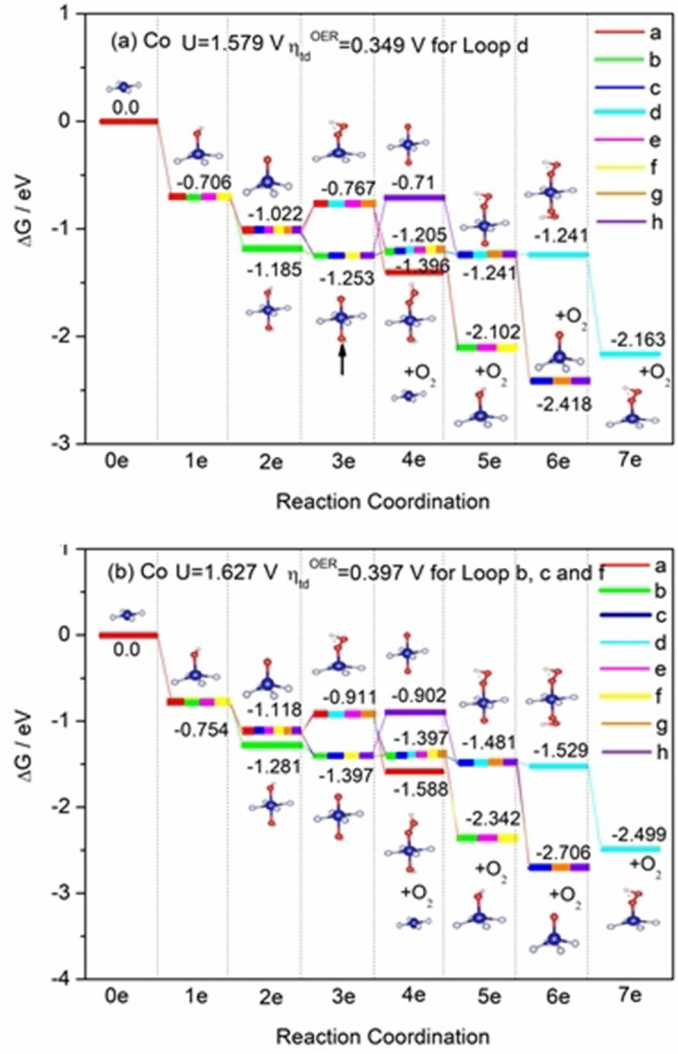

Figure 3. The free energy diagrams for the whole OER on Co@N_4TG under different potentials, the values of U and η^{OER} given at the top are from the loop indicated by bold lines, the TIS is indicated by a black arrow.

a′ is the actual active ORR loop for the whole reaction needs to be clarified by a TFLS plot and the plot is given in Figure 4(a) and (b). We can see from Figure (a) that, Loop d′, g′, h′ and c′ go uphill from *OOH + O_2 (at 1e) to *2OOH (at 2e), and from *O + O_2 (at 2e) to *1O1OOH (at 3e) under the potential of 0.837 V, respectively. The applied U would not make the above loops exothermic or adiabatic; Loop b′, e′, f′ and a′ share the common *OH + O_2 (at 3e). For Loop b′, e′ and f′, when they proceed from *OH + O_2 (at 3e) to the next step (at 4e), it is energetically more favorable for reaction to go towards * (at 4e) along Loop a′ . Thereafter, Loop a′ is proved to be the actual active ORR loop according to our RFLS plot.

The performance of the whole ORR loops under a lower reverse potential could be further tested. One can see from Figure 4(b) that at a lower potential of 0.682 V, Loop d′ goes uphill from *OOH + O_2 (at 1e) to *2OOH (at 2e). The transitions from *O + O_2 (at 2e) to *1O1OOH (at 3e) in Loop c′, g′ and h′ are endothermic. While for Loop e′, b′ and f′, they prefer to go along Loop a′ when going from *OH + O_2 (at 3e) to *1OH1OOH (at 4e). All in all, Loop a′ is confirmed as the active ORR loop for the whole reaction with an η_{td}^{ORR} of 0.357 V, and the rate-determining step is the last one from *OH to * + O_2.

We then conclude that Co@N_4TG turns out to be a highly promising electrocatalytic candidate for both OER and ORR with η_{td}^{OER} and η_{td}^{ORR} are 0.397 and 0.357 V, respectively. These over-potentials are much lower than those of the best catalysts identified theoretically 0.42 for OER on RuO_2 and 0.45 V for ORR on Pt metal.[14,30] The active OER loop is the Loop b in Figure 2 and it was omitted when only a single FERL starting from the ***bare*** Co site is considered. Therefore, the TFLS scheme should be employed in screening OER or ORR electrocatalyst when the reaction site might be multiply adsorbed by O, OH or OOH. Some other FERLs might show lower over-potential and act as the active reaction loop.

One must point out that a lower over-potential (about 0.2 ~ 0.3 V) from some single FERLs would not guarantee the whole reaction activity. As we will see below, reaction on Fe@N_4TG is such a good case.

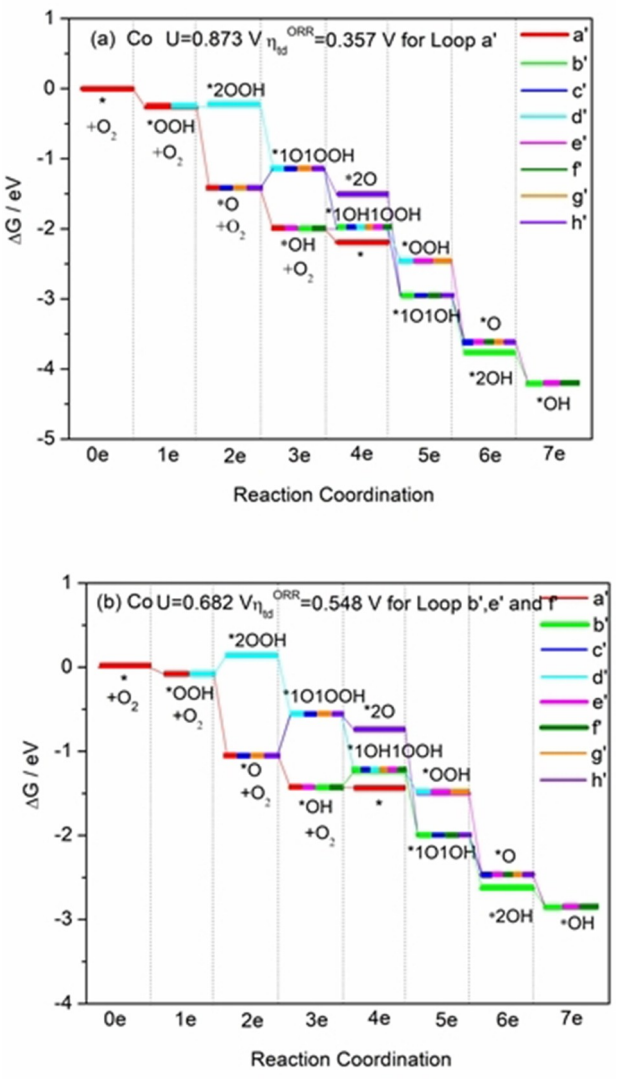

Figure 4. The free energy diagrams for the whole ORR on Co@N_4TG under different potentials, the values of U and η^{ORR} given at the top are from the loop indicated by bold lines.

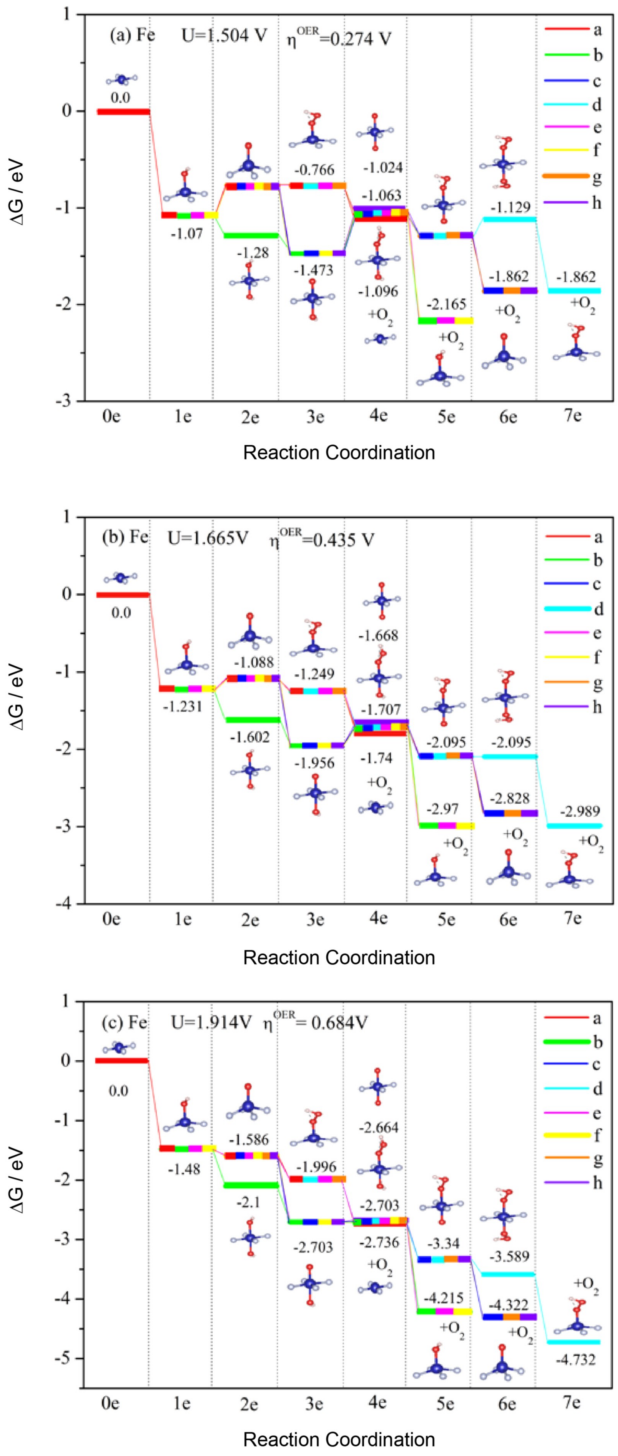

Figure 5. The free energy diagrams for all the successive OER FERLs of FeN_4TG under different potentials, the values of U and η^{OER} given at the top are from the loop indicated by bold lines.

Figure S3 lists the eight FERLs occurred on Fe@N_4TG. Figure S3(a) represents the OER/ORR loop that is usually employed in most theoretically screening work. The calculated η_{td}^{OER} (0.578 V)and η_{td}^{ORR} (0.796 V)from Loop a and a' indicate the poor performance of Fe@N_4TG used in water oxidation and fuel cells. Among the eight individual FERLs, the η_{td}^{OER} and η_{td}^{ORR} for Loop g and g' are notably as low as 0.274 and 0.298 V, respectively. These low overpotentials obtained from some **single** loop could not account for the **overall** performance of Fe@N_4TG towards OER and ORR. The TFLS plot for OER on FeN_4TG at 1.504 V is given in Figure 5(a). Such a potential confirms that the individual Loop g is operational since it has the most ideal η_{td}^{OER} of 0.274 V. As indicated by the bold orange bars in Figure 5(a), loop g starts from *O (at 2e) and prefers to proceed towards *OH (at 1e) rather *OOH (at 3e). The reason is that loop a, e, f and g share the intermediate state *O (at 2e) and much energy (about 0.304 eV) would be released if Loop g goes from *O (at 2e) to *OH (at 1e). As a potential TIS, the *OH (at 1e) would poison Loop a, e and f. When reaction goes back to *OH (at 1e), it will continue to go along Loop b and reach *2OH (at 2e), which is about 0.21 eV lower in energy than *OH (at 1e). Nevertheless, Loop b also encounters an energy barrier (0.41 eV) when it transits from *1O1OH (at 3e) to *1OH1OOH (at

4e), which means that the *1O1OH (at 3e) is also a TIS. Meanwhile, the *1O1OH (at 3e) will poison Loop c, f and h. When a larger U is applied to the system, these barriers will be lowered but still exist at the potential of 1.665 V (see Figure 5(b)). These energy barriers for transitions from *OH (at 1e) to *O (at 2e), and from *1O1OH (at 3e) to *1OH1OOH (at 4e) were lowered to be 0.143 eV and 0.249 eV, respectively. We then expect if an additional potential of 0.249 V (that is 1.914 V) were applied to the system, those TISs observed above would disappear. Figure 5(c) is the TFLS plot under 1.914 V and it shows that Loop b and f are the active individual FERLs. These two FERLs share some intermediate states (*OH (at 1e),*1O1OH (at 3e) and *1OH1OOH (at 4e)). From the perspective of the whole reaction, it is more favorable for reaction to proceed from *OH (at 1e) to *2OH (at 2e), as the latter transition releases much energy (about 0.62 eV). Therefore, the real active OER loop on Fe@N_4TG is Loop b, the corresponding η_{td}^{OER} is 0.684 V and the rate-determining step is the same as that in Co@N_4TG, indicating its poor electrocatalytic performance toward OER.

The ORR activity of Fe@N_4TG is further investigated by our TFLS plot. If individual FERL is considered, Loop g' gives the lowest η_{td}^{ORR} of 0.298 V as shown by Figure S3. From the TFLS plot in Figure 6(a), we can see that at a reverse electrode potential of 0.932 V, reaction will prefer to go along Loop a' rather Loop g' since the two loops share the intermediate state $*O+O_2$ (at 2e) and the energy of $*OH+O_2$ (at 3e) is much lower than that of *1O1OOH (at 3e). Nevertheless, Loop a' comes to an end since it has a higher energy barrier to surmount at 4e. Consequently, the applied U of 0.932 V will not make the whole system exhibit ORR activity. At a lower reverse potential of 0.797 V, Loop c' and h' could work individually. From the perspective of the whole reaction, reaction preferentially goes along Loop a' since Loop c' and h' also shares the intermediate state $*O+O_2$ (at 2e). Loop a' will also run into a barrier when it transits from $*OH+O_2$ (at 3e) to * (at 4e), and becomes the rate-determining step. An even lower potential U is needed to lower the barrier. All in all, the overall active ORR loop on Fe@N_4TG is Loop a' with an η_{td}^{ORR} of 0.797 V demonstrating the very poor potential for ORR.

We then come to the following conclusion: although some single FERL displays very low overpotential, it cannot ensure the catalytic activity of the whole reaction. Surely, if all the overpotentials of the eight consecutive FERLs that make up the whole reaction are very high, the catalyst will certainly show no catalytic activity. The Ni@N_4TG system is such a case. The free energy diagrams for all the eight individual FERLs on Ni@N_4TG and for all the successive OER/ORR FERLs on Ni@N_4TG under different potentials are given in Figure S4–S6. Figure S4 shows that none of the eight FERLs has potential OER or ORR activity. The TFLS plot for OER in Figure S5(a) under the lowest potential of 1.860 V indicates that Loop h starts from *O (at 2e), then goes to *OOH (at 3e) and it will proceed to *1OH1OOH (at 4e). The reason is that Loop h, b, c and f share the intermediate state *OOH (at 3e) and it is energetically favorable to go along this path. The reaction will go further towards $*OH+O_2$ (at 5e) along Loop b, e and f. Another cycle begins from *OH (at 1e). Then the reaction will proceed along Loop b and also Loop e and f. The latter two will encounter an energy barrier (0.189 eV) from *OH (at) to *O (at 2e). Although reaction continues along Loop b, it will meet another energy barrier (0.21 eV) from *2OH

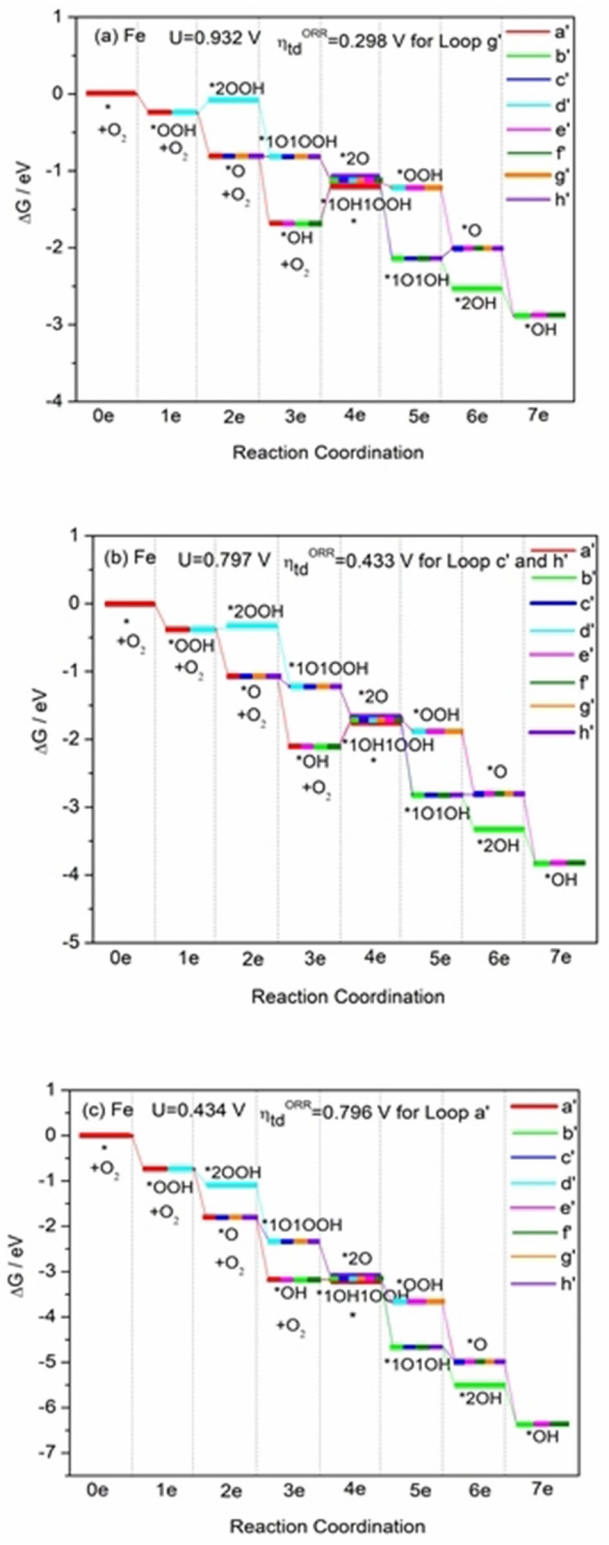

Figure 6. The free energy diagrams for all the successive ORR FERLs on Fe@N_4TG under different potentials, the values of U and η^{ORR} given at the top are from the loop indicated by bold lines.

(at 2e) to *OOH (at 3e). Hence, the intermediate state *2OH (at 2e) is the TIS of the whole reaction. An even larger potential is required to make the disappearance of this TIS. To activate Loop b, an energy of 2.07 eV is needed, which makes all the four elementary steps in Loop b downhill. Figure S5(b) gives the TFLM plot at a potential of 2.113 V, from where we can conclude that Loop b is the active OER loop for the whole reaction. The second reaction from *2OH to *1O1OH is the rate-determining step. Similarly, its overpotential is too high to make it a potential OER electrocatalyst.

As for the ORR activity on Ni@N_4TG, at a potential of 0.644 V, Loop b′, e′, f′ are all working individually as shown in Figure S4. However, the TFLM plot in Figure S6(a) shows that as Loop a′, b′ and f′ have the same intermediate state *OH + O_2 (at 3e), reaction will preferentially go along Loop a′. So, Loop a′ is proven the true ORR loop even a lower potential is applied (see Figure S6(b)) and the reaction from *O to *OOH is the rate-determining step. Nevertheless, Loop a′ has an η_{td}^{ORR} of 0.595 V confirming that Ni@N_4TG shows no electrocatalytic activity towards ORR.

3. Conclusions

In summary, we have designed single Co, Fe and Ni atom supported on N_4TG as promising electrocatalysts for OER and ORR by density functional theory calculations. A thermodynamic full-landscape method where the free energies diagrams of all the intermediate states were plotted according to their successive oxidization/reduction stages was employed. The way to determine the correct thermodynamic over-potential is to find the minimum/maximum potential where no TIS in the whole FLM plot for OER/ORR is observed. Our TFLM is an extension to the currently most employed CHE scheme starting from ***bare*** metal site. Our calculations showed that this procedure could give different over-potentials from the conventional CHE method. We found that Co@N_4TG exhibited relatively high performance for both OER and ORR from our TFLM scheme, while its potential OER activity might be omitted if the CHE method starting from ***bare*** TM site is employed. Fe- and Ni@N_4TG were confirmed to show neither OER nor ORR activity by both the CHE and our TFLM plot. The actual active reaction loops are screened by TFLM plots and turned out to be not always the FERL starting from the ***bare*** TM. Based on our results, N_4TG is a very promising support used for design high activity and low-cost electrocatalysts for catalytic applications. This work would open a new door for the development of non-noble metal bifunctional electrocatalysts for overall water splitting and also shed light on TG-supported nanomaterials as advanced catalysts. Our work calls for further experimental confirmation.

Acknowledgements

The authors greatly thank the Chinese Fundamental Research Funds for the Central Universities (Grant no. 2017XKQY094) and Jiangsu Overseas Visiting Scholar Program for University Prominent Young & Middle-aged Teachers and Presidents to support this work. The authors also greatly appreciate the computation resources given by the Advanced Analysis and Computation Center of CUMT for the award of CPU hours to accomplish this work.

Conflict of Interest

The authors declare no conflict of interest.

Keywords: density functional theory · doping · electrochemistry · ORR/OER · single-atom catalyst

[1] a) A. Stambouli, E. Traversa, *Renewable Sustainable Energy Rev.* **2002**, *6*, 433–455; b) G. Girishkumar, B. McCloskey, A. C. Luntz, S. Swanson, W. Wilcke, *J. Phys. Chem. Lett.* **2010**, *1*, 2193–2203; c) C. Zhu, Q. Shi, S. Feng, D. Du, Y. Lin, *ACS Energy Lett.* **2018**, *3,* 1713–1721; d) X. Wen, Q. Zhang, J. Guan, *Coord. Chem. Rev.* **2020**, *409*, 213214.
[2] a) Y. Qian, Z. Hu, X. Ge, S. Yang, Y. Peng, Z. Kang, Z. Liu, J. Lee, D. Zhao, *Carbon* **2016**, *111*, 641–650; b) T. Takeguchi, T. Yamanaka, H. Takahashi, H. Watanabe, T. Kuroki, H. Nakanishi, Y. Orikasa, Y. Uchimoto, H. Takano, N. Ohguri, M. Matsuda, T. Murota, K. Uosaki, W. Ueda, *J. Am. Chem. Soc.* **2013**, *135,* 11125–11130; c) Y. Zheng, J. Liu, J. Liang, M. Jaroniec, S. Qiao, *Energy Environ. Sci.* **2012**, *5*, 6717–6731.
[3] a) C. Sealy, *Mater. Today* **2008**, *11*, 65–68; b) J. Greeley, I. Stephens, A. Bandarenka, T. Johansson, H. Hansen, T. Jaramillo, J. Rossmeisl, I. Chorkendorff, J. Nørskov, *Nat. Chem.* **2009**, *1*, 552–556; c) S. Chu, A. Majumdar, *Nature* **2012**, *488*, 294–303; d) Q. Zhang, Z. Duan, Y. Wang, L. Li, B. Nan, J. Guan, *J. Mater. Chem. A* **2020**, *8*, 19665–19673.
[4] a) Y. Wang, J. Mao, X. Meng, L. Yu, D. Deng, X. Bao, *Chem. Rev.* **2019**, *119*, 1806–1854; b) X.-F. Yang, A. Wang, B. Qiao, J. Li, J. Liu, T. Zhang, *Acc. Chem. Res.* **2013**, *46,* 1740–1748; c) A. Alarawi, V. Ramalingam, J.-H. He, *Mater. Today* **2019**, *11*, 1–23.
[5] a) K. Novoselov, D. Andreeva, W. Ren, G. Shan, *Frontiers of Physics* **2019**, *14*, 13301; b) H. Jin, C. Guo, X. Liu, J. Liu, A. Vasileff, Y. Jiao, Y. Zheng, S.-Z. Qiao, *Chem. Rev.* **2018**, *118*, 6337-6408; c) Q. Zhang, J. Guan, *Adv. Funct. Mater.* **2020**, *30*, 2000768.
[6] P. Serp, C. Rivera-Cárcamo, *ChemCatChem* **2018**, *10*, 5058–5091.
[7] Y. Liu, G. Wang, Q. Huang, L. Guo, X. Chen, *Phys. Rev. Lett.* **2012**, *108*, 225505-1–225505-5.
[8] X. Sheng, H.-J. Cui, F. Ye, Q.-B. Yan, Q. Zheng, G. Su, *J. Appl. Phys.* **2012**, *112*.
[9] Y. L. Peng, Bingzhang, Chen, Shaowei, *Adv. Mater.* **2018**, *30*, 1801995 .
[10] a) X. Kong, Y. Huang, Q. Liu, *Carbon* **2017**, *123*, 558–564; b) T. He, S. K. M. G. Will, A. Du, *Small Methods* **2019**, 1800419; c) Q. Li, C. Yang, L. Wu, H. Wang, X. Cui, *J. Mater. Chem. A* **2018**, *7*, 5981–5990; d) H. Yu, Y. Xue, B. Huang, L. Hui, C. Zhang, Y. Fang, Y. Liu, Y. Zhao, H. Liu, Y. Li, *iScience* **2018**, *11*, 31–41.
[11] S. Li, J. Sun, J. Guan, *Chin. J. Catal.* **2021**, *42*, 511–556.
[12] a) X. Qiao, J. Jin, H. Fan, L. Cui, S. Ji, Y. Li, S. Liao, *Catalysts* **2018**, *8*, 275; b) L. Zhang, Y. Jia, G. Gao, R. Yan, N. Chen, J. Chen, M. T. Soo, B. Wood, D. Yang, A. Du, X. Yao, *Chem* **2018**, *4*, 285–297; c) A. Zitolo, V. Goellner, V. Armel, M. T. Sougrati, T. Mineva, L. Stievano, E. Fonda, F. Jaouen, *Nat. Mater.* **2015**, *14*, 937–942; d) Q. Zhang, Z. Duan, M. Li, J. Guan, *Chem. Commun. (Camb.)* **2020**, *56*, 794–797; e) L. Bai, Z. Duan, X. Wen, J. Guan, *J. Catal.* **2019**, *378*, 353–362.
[13] a) Y. Singh, S. Back, Y. Jung, *Phys. Chem. Chem. Phys.* **2018**, *20*, 21095–21104; b) Y. Wang, E. Song, W. Qiu, X. Zhao, Y. Zhou, J. Liu, W. Zhang, *Prog. Nat. Sci.* **2019**, *29*, 256–264.
[14] J. Nørskov, J. Rossmeisl, A. Logadottir, L. Lindqvist, J. Kitchin, T. Bligaard, H. Jonsson, *J. Phys. Chem. B* **2004**, *108*, 17886–17892.
[15] a) X. Li, P. Cui, W. Zhong, j. li, X. Wang, Z. Wang, J. Jiang, *Chem. Commun.* **2016**, *52*, 13233–13236; b) J. Safaei, N. Mohamed, M. F. Mohamad Noh, M. Soh, N. Ludin, M. Ibrahim, W. Isahak, M. A. Mat Teridi, *J. Mater. Chem. A* **2018**, *6*, 22346-22380; c) X. Zhang, A. Chen, Z. Zhang, M. Jiao, Z. Zhou, *J. Mater. Chem. A* **2018**, *6*, 11446–11452; d) Y. Zheng, Y. Jiao, Y. Zhu, Q. Cai, A. Vasileff, L. Li, Y. Han, Y. Chen, S. Qiao, *J. Am.*

Chem. Soc. **2017**, *139*, 3336–3339; e) Y. Zhou, G. Gao, J. Kang, W. Chu, L.-W. Wang, *J. Mater. Chem. A* **2019**, *7*, 12050–12059.
[16] Y. Zhou, G. Gao, Y. Li, W. Chu, L.-W. Wang, *Phys. Chem. Chem. Phys.* **2019**, *21*, 3024–3032.
[17] a) J. Rossmeisl, Z.-w. Qu, H. Zhu, G.-J. Kroes, J. Norskov, *J. Electroanal. Chem.* **2007**, *607*, 83–89; b) G. Gao, A. O'Mullane, A. Du, *ACS Catal.* **2016**, *7*, 494–500.
[18] a) G. Parkinson, *Catal. Lett.* **2019**, *149*, 1137–1146 ; b) Y.-F. Li, *ChemSusChem* **2019**, *12*, 1846–1857 ; c) A. E. Russell, *Phys. Chem. Chem. Phys.* **2008**, *10*, 3607–3608.
[19] G. Kresse, J. Furthmüller, *Phys. Rev. B* **1996**, *54*, 11169–11186 .
[20] P. E. Blochl, *Phys. Rev. B* **1994**, *50*, 17953–17979.
[21] J. Perdew, K. Burke, M. Ernzerhof, *Phys. Rev. Lett.* **1996**, *77*, 3865–3868.
[22] S. Grimme, J. Antony, S. Ehrlich, H. Krieg, *J. Chem. Phys.* **2010**, *132*, 154104-1–154104-19.
[23] K. Mathew, R. Sundararaman, K. Letchworth-Weaver, T. A. Arias, R. G. Hennig, *J. Chem. Phys.* **2014**, *140*, 084106-1–084106-8.
[24] H. Xu, D. Cheng, D. Cao, X. C. Zeng, *Nat. Catal.* **2018**, *1*, 339–348.
[25] a) S. Chen, J. Duan, M. Jaroniec, S.-Z. Qiao, *Adv. Mater.* **2014**, *26*, 2925–2930; b) T. V. Vineesh, M. Kumar, C. Takahashi, G. Kalita, S. Alwarappan, D. Pattanayak, T. Narayanan, *Adv. Energy Mater.* **2015**, *5*, 1500658; c) X. Zhang, S. Yu, H. Chen, W. Zheng, *RSC Adv.* **2015**, *5*, 82804–82812.
[26] X. Zhang, Z. Yang, Z. Lu, W. Wang, *Carbon* **2018**, *130*, 112–119.
[27] Y. Zhou, G. Gao, W. Chu, L.-W. Wang, *Nanoscale Adv.* **2020**, *2*, 710–716.
[28] S. Laha, Y. Lee, F. Podjaski, D. Weber, V. Duppel, L. Schoop, F. Pielnhofer, C. Scheurer, K. Küster, U. Starke, K. Reuter, B. Lotsch, *Adv. Energy Mater.* **2019**, *9*, 1803795.
[29] H. Fei, J. Dong, Y. Feng, C. Allen, C. Wan, B. Volosskiy, M. Li, Z. Zhao, Y. Wang, H. Sun, P. An, W. Chen, G. Zhiying, C. Lee, D. Chen, I. Shakir, M. Liu, T. Hu, Y. Li, Y. Huang, *Nat. Catal.* **2018**, *1*, 63–72.
[30] I. C. Man, H. Y. Su, F. Calle-Vallejo, H. A. Hansen, J. I. Martínez, N. G. Inoglu, J. Kitchin, T. F. Jaramillo, J. K. Nørskov, J. Rossmeisl, *ChemCatChem* **2011**, *3*, 1159–1165.

Manuscript received: November 12, 2020
Revised manuscript received: December 15, 2020